Kinetics of the $CaO/Ca(OH)_2$ hydration/dehydration reaction for thermochemical energy storage applications

Yolanda A. Criado*, Mónica Alonso, J. Carlos Abanades

Instituto Nacional del Carbón, CSIC-INCAR, C/ Francisco Pintado Fe, 26, 33011, Oviedo. Spain.

* Corresponding Author: Tel: +34 985119090; Fax: +34 985297662; e-mail: yolanda.ac@incar.csic.es

Abstract

The calcium oxide hydration/dehydration reaction is proposed as a suitable reaction couple for thermochemical energy storage systems. However, limited work has been reported on the reaction kinetics of $CaO/Ca(OH)_2$ under appropriate operation conditions for storage applications involving fluidized beds. This study focuses on the effect of temperature, partial steam pressure and particle size upon the intrinsic hydration and dehydration reaction kinetics when natural materials are used. The experimental data have been fitted satisfactorily to a shrinking core model for both hydration and dehydration reactions, at reaction temperatures between 400 and 560ºC and partial steam pressures between 0 and 100kPa. The reaction rates measured are higher than those previously reported in the literature. In the case of large particle sizes of natural material, particle attrition has been detected indicating the need to develop more suitable materials for thermochemical energy storage applications.

Introduction

Thermal energy storage (TES) systems at large scale are a key component for increasing the reliability, dispatchability and efficiency of thermal solar power plants, as they allow the power production profile of the solar field to be adapted to demand[1-3]. The main types of TES technologies available for solar energy systems are sensible heat storage (by solid or liquid media, see Gil et al.[4]), latent heat storage (mainly in the solid-liquid phase transition, see Liu et al.[5]), sorption heat storage (physical or chemical) and heat storage by reversible chemical reactions [1, 4, 6]. The last two technologies are known as thermochemical energy storage and, in theory, they would yield the highest storage energy densities, although they are still at the R&D stage.

The hydration/dehydration of CaO (reaction 1) is considered as a suitable reversible reaction for thermochemical energy storage systems[6], as the reaction enthalpy is high (-104 kJ/mol) and energy can be released during the hydration (discharging step) and stored during the dehydration (charging step). The temperature level at which the heat can be released (450-500ºC) facilitates the thermal integration of the storage system within the solar field[3]. Furthermore, the reactants are easily storable, stable, low cost and environmentally friendly[7].

$$CaO\ (s) + H_2O\ (g) \leftrightarrow Ca(OH)_2\ (s) \quad \Delta H_{298K} = -104\ kJ/mol \qquad (1)$$

The reactors traditionally considered suitable for the hydration and dehydration reactions in a thermochemical energy storage system coupled to a solar field are fixed beds[8-13]. However, fixed beds have inherent limitations in terms of heat transfer efficiency. The inherently low thermal conductivity of stationary solids necessitates a very large network of heat transfer surface from which the large amount of thermal power required for a large-scale system needs to be extracted and transferred. Also, high

pressure drops in the reacting gases (steam during hydration and/or air during dehydration) would be required in the storage vessel to put the fine particle solids into contact with the reacting or purge gases. If large pellets or particles are used to minimize these effects, the reaction kinetics can become very slow and mechanical stresses produced during the reaction may lead to pellet or particle breakage. Fluidized bed reactor systems using CaO particles (or CaO-supported particles on an inert and easy-to-fluidize ceramic support) are an alternative option for carrying out hydration and dehydration reactions. These systems can operate in continuous mode and the heat transfer coefficients to internal surfaces in the reactor are very high, which means that the heat transfer area requirements in fluidized beds are considerably reduced. Also, operations such as the separation of gases and solids, the feeding or extraction of solids and their handling and transport to and from the storage silos can draw on the experience of many similar systems in the chemical and energy industry. Circulating or bubbling fluidized beds for the hydration/dehydration of $CaO/Ca(OH)_2$ had already been recognized as possible reactor choices in the pioneering works of Ervin[14, 15] and Rosemary et al.[16] as far back as the 70's. However, no further progress has been made since then in the development of these reactor concepts.

Within the framework of a recent EU funded project StoRRe (www.storre.eu) we are investigating the applicability of fluidized bed reactors to thermochemical energy storage systems using the $CaO/Ca(OH)_2$ reversible reaction. The basic process concept proposed by CEA for this project is represented in Figure 1. In this process, in-coming heat (from the solar field or any other heat source) is used to dehydrate the $Ca(OH)_2$ that decomposes into CaO (which is then stored) and steam. A small fraction of air may be used as fluidizing gas, although the steam produced during the dehydration of the incoming solid flow could be sufficient to sustain most of the fluidization of the solids.

During the hydration stage, useful heat is released in the reactor when the CaO is re-hydrated by the reaction with the steam (which also acts as fluidizing gas).

An essential part of the design of the thermochemical energy storage system in Figure 1 is the intrinsic reaction kinetics of the CaO hydration and $Ca(OH)_2$ dehydration under realistic operating conditions (reaction atmospheres and temperatures). Although some works have investigated direct hydration with liquid water [17-19], hydration must be carried out with steam because otherwise the efficiency of the energy storage is severely reduced ("Heat out" arrow in Figure 1): the hydration enthalpy decreases from - 104 to - 62kJ/mol in standard conditions when liquid water is used as a reactant instead of steam.

Although CaO hydration/dehydration reactions have been previously recognized as a suitable thermochemical energy storage system, only a few works have focused on the experimental evaluation of the kinetics of these reactions [18-27] and in most cases the operating conditions do not match the requirements of a storage system such as that described in Figure 1.

A recent work by Schaube et al.[20] evaluated the hydration and dehydration reaction kinetics at high partial steam pressure (up to 95.6kPa) over a large number of hydration-dehydration cycles and their material did not display any significant degradation up to 100 cycles. They used different empirical kinetic models for each reaction step depending on the operation temperature during hydration and depending on whether the dehydration conversion was higher or lower than 0.2. Lin et al. and Wang et al.[21-23] also recently evaluated the kinetics of the CaO hydration/$Ca(OH)_2$ decomposition at high temperature (550-710ºC) and high partial steam pressure (0.67-2.33MPa for hydration and a total pressure of 1-3.5MPa) over several cycles. However,

the temperature and pressure values at which the reaction kinetics were evaluated in these works are outside the range (very high pressures) of interest for a process aimed at fluidized bed technology operating at atmospheric pressure as in Figure 1. Irabien et al.[24] obtained a kinetic model for the dehydration of calcium oxide in the range of temperatures of 330-450ºC using the random pore model and proposed a pseudo-homogeneous kinetic model to describe the behavior of calcium hydroxide during the dehydration process. However, they reported that with their experimental system the influence of external mass transfer and particle diffusion could not be easily avoided. Hydration kinetics under liquid water [18, 19] instead of steam as proposed by Irabien et al. in another work, are not applicable to thermochemical energy storage processes for the reasons mentioned above. Galwey et al.[25] studied the dehydration reaction in a glass vacuum apparatus coupled to a TG analyzer using 10mg and 28mg samples of $Ca(OH)_2$. Their study showed that dehydration rates were affected by the dispersion of the reactant particles inside the reaction tube in an ideal fixed bed. They found that a first order rate equation provided the most satisfactory fit to the data. Over successive dehydration/rehydration cycles they observed that reaction rates increased in both directions as a result of crystallite disintegration, with the reaction proceeding more rapidly for smaller particles. Matsuda et al.[26] studied the reversible $Ca(OH)_2$/CaO reaction for energy storage applications at reaction temperatures between 83 and 450ºC and steam concentrations between 1.5 to 15.7%vol. and proposed a first order reaction for both reactions. However, the partial steam pressure applied in their work was substantially lower than what would be used in systems such as that of Figure 1, where a maximum steam content in the gases is targeted in order to minimize the air flow requirement and hence, the cross-sectional area of the reactors for a given superficial gas velocity.

In view of the limited research work carried out on CaO hydration/dehydration reactions kinetics for thermochemical energy storage applications with particle materials suitable for fluidized bed reactors, the aim of this work is to study the intrinsic kinetics of the hydration and dehydration reactions of CaO in highly concentrated atmospheres of steam. The kinetics information obtained and the model used to interpret the experimental results will be a valuable tool for designing fluidized bed reactors for use in energy storage systems such as that represented in Figure 1. The materials and experimental conditions for the kinetic experimental tests have been selected with this aim in mind.

Experimental Section

The hydration and dehydration reactions of CaO particles have been experimentally studied in a thermo-gravimetric analyzer (TG) especially designed for long multicycle gas-solid reactions, and adapted to operate with pure steam or air-steam mixtures, as described below.

The TG apparatus consists of a quartz tube (2.5×10^{-2}m o.d.) placed inside a two-zone furnace capable of working at temperatures of up to 1000ºC and at different temperatures in each furnace zone. For the tests described in this work, the sample holder was located in the upper furnace position, allowing the bottom part of the oven to be used for preheating and mixing the steam and air mixture before they reached the sample. During all the experiments, the sample weight, temperature and flows were continuously recorded on a computer.

For each run in the TG, around 3 mg of sample was introduced into the sample holder and the total gas flow was set to 7.3×10^{-6}m^3/s (STP) which corresponds to a superficial gas velocity of 0.05m/s around the sample at 550ºC. This avoids undesired diffusional

effects around the sample when a high amount of mass and/or low gas velocities are used. In these conditions the kinetics observed during the experiments will be representative of the intrinsic characteristics of hydration/dehydration reactions and not of the particular characteristics of the experimental set up (shape and size of the plate, reacting gas velocity, location of thermocouple etc.) or the sample (i.e. sample mass). The high gas velocity, required to derive relevant kinetic parameters at particle level, caused some disturbances in the weight readings in the TG head, that need to be calibrated. To determine the additional disturbances in the weight readings when changing from hydration to dehydration, blank experiments for each different set of conditions were performed using an empty sample holder and an inert material. After correcting the data obtained from the blank tests, plots of conversion vs. time for each cycle were made from the weight losses and gains recorded. At the end of each run, the samples were weighed in a different precision balance to check the accuracy of the weight measurements made during the experiments.

The TG system used in this work is depicted in Figure 2. The bottles on the left-hand side of the figure contain one liter of distilled liquid water at ambient temperature and pressurized to 500kPa by means of N_2. Two parallel lines of water were installed in order allow a continuous supply of water to the system. After the water bottles, a *Bronkhorst* liquid mass flow controller provides a precise water mass flow of between 1.4×10^{-3} and 2.8×10^{-2}g/s. To vaporize the liquid water, the pipeline is heated by means of a heating tape whose temperature (the same as the oven temperature to avoid changes in the steam flow between the pipe line and the TG) is adjusted by means of a temperature controller. This heating zone is located at a sufficient distance from the mass flow controller (0.2m) to ensure that the high temperature does not interfere with the controller. To guarantee complete, uniform and stable vaporization in the first

heating zone, several filters are situated along the pipe line to ensure a uniform distribution of the water. After the filters, a precision needle valve creates a damping effect when combined with the water bottles pressurized to 500kPa. This ensures that a continuous and steady flow of steam is provided to the TG.

A three-position pneumatic valve allows a continuous flow of steam during the change from steam (or mixtures of air and steam) to air conditions. The valve inlet is connected to the heated steam generation pipe. One of the valve outlets is connected to the TG apparatus inlet pipe line (also heated up) and the other one to a cold pipe where steam is condensed before it leaves the system. During the pure steam or air-steam mixture step, the pneumatic valve inlet is connected to the TG and during the pure air step the steam leaves the system through the cold pipe.

Steam and/or synthetic air are fed to the bottom of the quartz tube enclosed by the oven. Up to the oven, the pipe connected to the quartz tube is also heated up. The low furnace zone (below the sample basket) is heated up to the lower experimental temperature. The temperature in the upper zone was selected as the reaction temperature for the hydration and dehydration conditions respectively. To minimize errors arising from the temperature profiles in the oven, the sample temperature is controlled by a thermocouple located just a couple of millimeters below the sample pan. To allow the gas to leave through the orifice at the top of the quartz tube, a continuous air purge is passed through the balance head ($3.3\times10^{-5}m^3/s$ (STP)). The top of the quartz tube is also heated up to 50ºC by means of a thermal cord.

For the hydration/dehydration cycling experiments, CaO was obtained from two natural limestones with different compositions, Compostilla (89% $CaCO_3$) and Imeco (98.7% $CaCO_3$) that were calcined at 800ºC in pure air ($7.3\times10^{-6}m^3/s$ (STP)) for 10 min before

each experiment. A series of tests were carried out to determine the effect of the particle size on the hydration/dehydration rates. For this purpose four particle size cuts were tested 100-200μm, 400-600μm, 800μm-1mm and 1-2mm. Since the main objective of this work is to derive intrinsic hydration/dehydration kinetics, the 100-200μm particle size was used in most tests. The hydration and dehydration reactions were studied over a temperature range of 400 to 560ºC and several partial steam pressures (P_{H2O}) were tested ranging from pure steam to pure air at a total pressure of 100kPa.

Results and Discussion

Most of the experiments carried out to derive kinetic data for the hydration and dehydration reactions considered in this work have been conducted in conditions relatively close to equilibrium. This is because the design of energy storage systems used to exploit these reversible reactions aims to operate at the highest possible temperature in the case of hydration (to maximize the efficiency in the transformation to useful energy of the "Heat out" arrow of Figure 1). This will lead to operation conditions close to the equilibrium for hydration (at atmospheric pressure, this means temperatures in the range of 450 to 500ºC in steam volume fractions close to one). In contrast, for the dehydration step, the design aims to operate at the lowest possible temperature (to minimize the heat requirements for preheating the solids and the dehydration reaction). In principle, this can be achieved by two means: using a large flow of purge gas (air or equivalent) in order to operate the dehydrator under low volume fractions of steam or using dehydration temperatures as close as possible over the equilibrium. The first approach requires a larger flow of air in Figure 1, which will increase the energy required to heat up the gas and the gas velocities in the fluidized bed dehydrator reactor. The second approach (minimum or no air requirements) will require operation at temperatures close to the equilibrium temperature (between 500 to 550ºC).

These design decisions (in particular the one affecting the flow of air to the dehydrator) will have large implications for the required reactor design (bubbling reactors vs. circulating fluidized bed reactors) but detailed analysis of these reactors is beyond the scope of this paper. What is clear from the previous discussion is that in all cases, both the hydration and dehydration reactions will be conducted in conditions as close as possible (kinetics allowing) to the equilibrium of $H_2O(v)$ in CaO.

The $CaO/Ca(OH)_2$ equilibrium curves available in the literature give different temperatures over the temperature range studied in this work. As can be seen in Figure 3, predictions from thermo-chemical data provided by Barin[28] and Nikulshina[29] give an equilibrium temperature of 519 and 514ºC respectively for pure steam at atmospheric pressure, compared to the curves experimentally obtained by Samms and Evans[30], Schaube et al.[20] and Halstead and Moore[31] who obtained values between 505-510ºC. Experimental measurements of the equilibrium were performed in the TG experimental facility described in the experimental section to detect the temperature at which $Ca(OH)_2$ (obtained from the hydration of CaO at 450ºC and a partial steam pressure of 100kPa) dehydrates by increasing the temperature (rate of 2ºC/min) while maintaining the partial steam pressure. This experiment was repeated for three different partial steam pressures, 100, 75 and 50kPa. These tests yielded equilibrium temperatures very close to those predicted from thermo-chemical data provided by Barin ENREF 25 (518, 508 and 488ºC for P_{H2O} of 100, 75 and 50kPa respectively in our work). Therefore, for the kinetic model described below, equation (2) obtained by fitting data from Barin[28] will be adopted:

$$P_{eq} = 2.30 \cdot 10^{8} \cdot \exp\left(-\frac{11607}{T}\right) \qquad (2)$$

Experimental curves of hydration conversion (X_{Hy}) vs. time were obtained for CaO samples of different particle size (diameter ranges between 0.1 and 2mm), at various volume fractions of steam (from 0.5 to 1) and temperatures (between 400 and 500ºC). Figure 4 shows the experimental results for the CaO hydration conversion at different partial steam pressures (100, 75, 65 and 50kPa). The results shown here correspond to the calcined Compostilla limestone (89% $CaCO_3$). However, tests were also performed using Imeco (98.7% $CaCO_3$) and similar results were obtained for both samples.

As can be seen in Figure 4, after a fast initial kinetic regime there is a smooth change in the reaction rate to a slower reaction regime. The experimental results show that complete conversion can be achieved within 20-30s under high partial steam pressures (i.e. 100 or 75kPa) which are the most favorable hydration conditions for these experiments. The fluctuations in hydration conversion between 0.85-1 are attributed to inherent experimental measurement errors, as no-similar trend has been observed in other experiments. These experimental results reveal a much faster hydration reaction than expected when compared to the kinetic results described by other authors in the state of the art [20, 21, 26]. As pointed out in the experimental section, special care was taken to minimize diffusional resistances related to the experimental setup, gas solid flows or sample mass. The absence of these resistances during the kinetic reaction test could explain why the rate of the hydration reactions in Figure 4 is somewhat higher than expected.

Another important consequence of the results in Figure 4 is that the hydration rates can be expressed as a first order reaction with respect to the steam volume fraction (ν_{H2O}) or steam partial pressure:

$$\frac{dX_{Hy}}{dt} = k_{Hy}(T)\cdot(\nu_{H2O} - \nu_{eq})\cdot f(X_{Hy}) \qquad (3)$$

This dependency has been observed in other series of experiments similar to those of Figure 4 and is quite common in reversible decomposition reactions [32].

The temperature dependence of the kinetic constant $k_{Hy}(T)$ was estimated by fitting individual values of k_{Hy} data at different temperatures, as shown in Figure 5. The activation energy for the CaO hydration derived from these results is $E_{Hy}=(59.4\pm0.5)\times10^3$J/mol and the pre-exponential factor is $A_{Hy}=(2.5\pm0.2)\times10^{-6}$ 1/s. The activation energy value obtained is consistent with the range of values reported in the literature[20] between 58.2×10^3 and 83.5×10^3J/mol. _ENREF_15

Finally, experiments with different particle sizes were carried out to identify the reaction surface available during hydration and the overall reaction model at particle level. Two extreme reaction models were considered depending on whether the reaction occurred throughout the entire particle at the same time -a pseudo-homogenous model- or whether the reaction occurred on the particle surface -shrinking core model-[33].

Figure 6 represents the results of these experiments in terms of maximum reaction rate (experimental $\Delta X_{Hy}/\Delta t$) vs. the inverse of the average particle diameter (dp). The same operation conditions were maintained for each particle size interval. As can be seen, the results fit to a straight line, which points to a shrinking core model in which the chemical reaction is the controlling stage (at least during the first fast stage of the hydration reaction). Therefore, assuming spherical particles, equation (4) can be applied to calculate the CaO hydration conversion as a function of time as follows:

$$\frac{dX_{Hy}}{dt} = \frac{1}{dp}\cdot A'_{Hy}\cdot \exp\left(\frac{E_{Hy}}{R\cdot T}\right)\cdot(v_{H2O} \quad v_{eq})\cdot 3(1 \quad X_{Hy})^{2/3} \qquad (4)$$

and in integrated form:

$$X_{Hy} = 1 - \left(1 - \frac{t}{\tau_{Hy}}\right)^3 \quad (5)$$

where the complete hydration conversion time (τ_{Hy}) is:

$$\tau_{Hy} = 1 \Big/ \left[\frac{1}{d_p} \cdot 3.5 \cdot 10^{-4} \cdot \exp\left(\frac{59.4 \cdot 10^3}{R \cdot T}\right) \cdot (v_{H2O} - v_{eq})\right] \quad (6)$$

As confirmation of the satisfactory fit of the results, the dotted lines in Figure 4 were plotted using equations (5) and (6) with the parameters derived from Figures 5 and 6.

For the dehydration reaction experiments, the same fitting procedure as for hydration was followed. Firstly, the effect of the partial steam pressure on the dehydration reaction was evaluated as in the example of Figure 7, in which the dehydration conversion (X_{Dehy}) is represented vs. time at partial steam pressures ranging from pure air to 100kPa for Compostilla limestone (tests using Imeco limestone yielded similar results as in the case of the hydration reaction) of 100-200μm particle size. As can be seen, when the dehydration reaction takes place under pure air (0kPa) at 500ºC, decomposition rates are very fast and complete dehydration is achieved in less than 30s. Even when the partial steam pressure is slightly increased (i.e. 10 or 25kPa) the reaction rates are much faster than expected compared to the results reported in the literature [20, 24, 26]. However, as discussed in the previous sections, it is not realistic to expect such a low partial pressure of steam during the dehydration of $Ca(OH)_2$ particles in a fluidized bed reactor such that of Figure 1. This is because in large scale systems (aimed at releasing tens of MWt of thermal power during hydration), the flow of $Ca(OH)_2$ will necessarily have to be very high during the dehydration periods in order to charge the silos with CaO. This means that the molar flow of steam coming from the dehydrator reactor will also be very high. Therefore, in order to operate this reactor at low steam

partial pressures, (for example P_{H2O}=10kPa) it will be necessary to use an air flow 10 times higher than the steam flow coming out of the reactor. This will entail large energy requirements and additional equipment for preheating the air as well as unacceptable large reactor cross-sections and/or superficial gas velocities. Therefore, the most useful kinetic information for dehydration must be obtained at higher partial pressures of steam.

As can be seen in Figure 7, as the partial steam pressure increases and the operation conditions approach equilibrium (for a partial steam pressure of 50kPa) the reaction rates slow down considerably. On the other hand, as discussed above, future reactors may have to operate for dehydration under pure steam at the expense of higher reactor temperatures. In this example, this is represented by a single curve at 560ºC (see Figure 7), which indicates that $Ca(OH)_2$ dehydrates completely within only 10s under these conditions, far from the equilibrium due to the higher operating temperature.

As in the case of the hydration reaction, the dehydration reaction fits well to a first order reaction:

$$\frac{dX_{Dehy}}{dt} = k_{Dehy}(T)\cdot(v_{eq} - v_{H2O})\cdot f(X_{Dehy}) \qquad (7)$$

The temperature dependence of the kinetic constant $k_{Dehy}(T)$ was also estimated by fitting the individual values of k_{Dehy} data at different temperatures as shown in Figure 8 for dehydration experiments under air at different temperatures. In this case the Arrhenius parameters for the dehydration reaction derived from the experimental data are an activation energy of $E_{Dehy}=(60.8\pm0.3)\times10^3$J/mol and a pre-exponential factor of $A_{Dehy}=(5.2\pm0.6)\times10^2$ 1/s. The activation energy calculated is in the range of values reported in the literature between 30 and 190×10^3J/mol [25].

For the dehydration reaction, tests were also conducted using different particle sizes in order to find the appropriate overall reaction model at particle level and the relevant reaction surface during dehydration. As in the case of the hydration reaction, Figure 9 shows these experiments results by means of the values of maximum reaction rate (experimental $\Delta X_{Dehy}/\Delta t$) vs. the inverse of the average particle diameter (dp) while maintaining the same operation conditions for each particle size tested. As can be seen the results fit to a straight line, the maximum reaction rate decreases linearly with the particle size. Therefore a shrinking core model in which the chemical reaction is the controlling stage is also proposed for the dehydration. Again, assuming the particles to be spherical, the $Ca(OH)_2$ dehydration conversion as function of time can be calculated using equation (8) as follows:

$$\frac{dX_{Dehy}}{dt} = \frac{1}{dp} \cdot A'_{Dehy} \cdot \exp\left(-\frac{E_{Dehy}}{R \cdot T}\right) \cdot (v_{eq} - v_{H2O}) \cdot 3\left(1 - X_{Dehy}\right)^{2/3} \quad (8)$$

or in integrated form:

$$X_{Dehy} = \left(1 - \frac{t}{\tau_{Dehy}}\right)^3 \quad (9)$$

where the complete dehydration conversion time (τ_{Dehy}) is calculated using equation (10):

$$\tau_{Dehy} = 1 \Big/ \left[\frac{1}{dp} \cdot 7.3 \cdot 10^4 \cdot \exp\left(-\frac{60.8 \cdot 10^3}{R \cdot T}\right) \cdot (v_{eq} - v_{H2O})\right] \quad (10)$$

The dotted lines in Figure 7 were also plotted using equations (9) and (10) with the parameters derived from Figures 8 and 9, confirming that the X_{Dehy} vs. time curves calculated from these equations adjust reasonably well to the experimental results.

Finally, several experiments were conducted in which individual samples of different particle size were subjected to several cycles of hydration and dehydration.

Figure 10 shows the hydration conversion (X_{Hy}) vs. the number of cycles of hydration-dehydration (N) for experiments carried out with hydration during 300s at 450ºC and P_{H2O}=65kPa followed by complete dehydration at 500ºC in pure air. As can be seen, for the smaller particle size intervals (100-200μm and even for 400-600μm) almost total hydration is achieved in all the cycles after 300s. Further tests up to 32 cycles with calcined natural limestone of size 100-200μm showed no decay in hydration/dehydration conversion, confirming the reversibility of the reaction couple (in agreement with the experimental results reported by Ervin[14] and Rosemary et al.[16] up to 211 and 1171 cycles respectively). However, as the particle size increases (800μm-1mm and 1-2mm) no complete hydration conversion is achieved after 300s during the first few hydration cycles. This result is fully consistent with the shrinking core model described above, as the available surface is inversely proportional to the particle size (Figure 6) and 300s is too short time to achieve higher conversions than those reported in Figure 10. However, a clear trend towards increasing conversion with the number of cycles is observed, which may be related to physical damage and the breakage of the particle porous structure with the consecutive hydrations and dehydrations, confirmed by visual observation of the particles after these tests. The particle breaking mechanism facilitates the diffusion of steam through the particle cracks and makes more CaO surface available for reaction with steam.

When the largest particle size cuts were subjected to higher partial steam pressure during hydration (>75kPa) at a temperature of 450ºC, the particles were completely broken down into fine powders after the first or second cycle and complete conversion were achieved in all the cycles in just a few seconds as were observed with the 100-

200μm size cut. These experiments at higher pressure gradients during hydration show that the use of high partial steam pressure and the fast hydration rate are counterproductive because the mechanical resistance diminishes as the hydration rate increases. The particle breakage observed indicates that there is scope for optimizing hydration conditions in order to minimize material losses. It will probably be necessary to use CaO-supported or pretreated particles with better mechanical properties for fluidization. It is beyond the scope of the present work to analyze these materials. However the experimental and modeling results presented in this work to describe the kinetics of hydration and dehydration of $CaO/Ca(OH)_2$ should serve as a valuable aid for future designs of reactor concepts suitable for exploiting the energy storage potential of the $CaO/Ca(OH)_2$ hydration and dehydration reactions.

Conclusions

In this work the CaO hydration and $Ca(OH)_2$ dehydration reactions have been studied in the 400 to 560ºC temperature range and at partial steam pressures from 0 to 100kPa in a thermo-gravimetric analyzer (TG) operating under differential conditions. These reaction conditions may be relevant to future designs of large scale thermochemical energy storage systems involving fluidized bed reactors for hydration and dehydration. The shrinking core model has been used to fit both the experimental hydration and dehydration conversion curves. The CaO particles react following a chemically controlled first order reaction, displaying activation energies of 59.4×10^3 and 60.8×10^3J/mol and pre-exponential factors of 2.5×10^{-6} and 5.2×10^2 1/s (for a particle size of 100-200μm) for hydration and dehydration reactions respectively. The reaction rates observed in all cases are considerably higher than the few so far reported in the literature under comparable conditions. This may indicate the presence of misleading

resistances to the progression of the reactions in previous studies. In this work, particle breakage has been detected when working with larger CaO particles, which indicates that it might be necessary to use CaO-supported particles with better mechanical properties for fluidization. However, since the reaction rates observed under reasonable reaction conditions were much faster than expected (complete hydration or dehydration was reached in less than 60s in most cases), it can be concluded that there is still scope for developing suitable materials and fluidized bed reactors to perform $CaO/Ca(OH)_2$ hydration and dehydration reactions in future energy storage systems .

Acknowledgment

The authors acknowledge the financial support provided by the European Commission under the 7th Framework Program (StoRRe Project GA 282677). Y.A. Criado thanks the Government of the Principality of Asturias for a Ph.D. fellowship (Severo Ochoa Program).

Nomenclature

A pre-exponential factor for a particle size cut of 100-200μm, 1/s

A' pre-exponential factor, μm /s

dp average particle size, μm

E activation energy, J/mol

k kinetic constant, 1/s

N number of hydration-dehydration cycles

P_{eq} equilibrium pressure, kPa

P_{H2O} partial steam pressure, kPa

R universal gas constant, J/mol K

T temperature, K

t time, s

X conversion, mol H_2O/ mol CaO

ΔH reaction enthalpy, kJ/mol at 298K

ν_{H2O} steam volume fraction

ν_{eq} equilibrium volume fraction

τ complete conversion time, s

Subscripts

Hy hydration reaction

Dehy dehydration reaction

References

(1) IPCC *Special Report on Renewable Energy Sources and Climate Change Mitigation*; Cambridge University Press: United Kingdom and New York, NY, USA, 2011.

(2) Hou, Y.; Vidu, R.; Stroeve, P. Solar Energy Storage Methods. *Ind. Eng. Chem. Res.* **2011,** 50, 8954-8964.

(3) Kuravi, S.; Trahan, J.; Goswami, D. Y.; Rahman, M. M.; Stefanakos, E. K. Thermal energy storage technologies and systems for concentrating solar power plants. *Prog. Energy Combust. Sci.* **2013,** 39, 285-319.

(4) Gil, A.; Medrano, M.; Martorell, I.; Lázaro, A.; Dolado, P.; Zalba, B.; Cabeza, L. F. State of the art on high temperature thermal energy storage for power generation. Part 1—Concepts, materials and modellization. *Renewable Sustainable Energy Rev.* **2010,** 14, 31-55.

(5) Liu, M.; Saman, W.; Bruno, F. Review on storage materials and thermal performance enhancement techniques for high temperature phase change thermal storage systems. *Renewable Sustainable Energy Rev.* **2012,** 16, 2118-2132.

(6) Cot-Gores, J.; Castell, A.; Cabeza, L. F. Thermochemical energy storage and conversion: A-state-of-the-art review of the experimental research under practical conditions. *Renewable Sustainable Energy Rev.* **2012,** 16, 5207-5224.

(7) Wentworth, W. E.; Chen, E. Simple thermal decomposition reactions for storage of solar thermal energy. *Sol. Energy* **1976,** 18, 205-214.

(8) Fujii, I.; Tsuchiya, K.; Higano, M.; Yamada, J. Studies of an energy storage system by use of the reversible chemical reaction: $CaO + H_2O \rightleftharpoons Ca(OH)_2$. *Sol. Energy* **1985,** 34, 367-377.

(9) Kanzawa, A.; Arai, Y. Thermal energy storage by the chemical reaction augmentation of heat transfer and thermal decomposition in the $CaO/Ca(OH)_2$ powder. *Sol. Energy* **1981,** 27, 289-294.

(10) Schaube, F.; Kohzer, A.; Schütz, J.; Wörner, A.; Müller-Steinhagen, H. De- and rehydration of $Ca(OH)_2$ in a reactor with direct heat transfer for thermo-chemical heat storage. Part A: Experimental results. *Chem. Eng. Res. Des.* **2013,** 91, 856-864.

(11) Schaube, F.; Utz, I.; Wörner, A.; Müller-Steinhagen, H. De- and rehydration of $Ca(OH)_2$ in a reactor with direct heat transfer for thermo-chemical heat storage. Part B: Validation of model. *Chem. Eng. Res. Des.* **2013,** 91, 865-873.

(12) Schaube, F.; Worner, A.; Tamme, R. High Temperature Thermochemical Heat Storage for Concentrated Solar Power Using Gas-Solid Reactions. *J. Sol. Energy Eng.* **2011,** 133, 031006.

(13) Schmidt, M.; Szczukowski, C.; Roßkopf, C.; Linder, M.; Wörner, A. Experimental results of a 10 kW high temperature thermochemical storage reactor based on calcium hydroxide. *Appl. Therm. Eng.* **2014,** 62, 553-559.

(14) Ervin, G. Solar heat storage using chemical reactions. *J. Solid State Chem.* **1977,** 22, 51-61.

(15) Ervin, G. Method of storing and releasing thermal energy. US 3.973.552, Aug. 10, 1976.

(16) Rosemary, J. K.; Bauerle, G. L.; Springer, T. H. Solar energy storage using reversible hydration/dehydration of $CaO\text{-}Ca(OH)_2$, AIAA Terrestrial Energy Systems Conference, Orlando, Florida, 1979; 79-0986.

(17) Azpiazu, M. N.; Morquillas, J. M.; Vazquez, A. Heat recovery from a thermal energy storage based on the $Ca(OH)_2/CaO$ cycle. *Appl. Therm. Eng.* **2003,** 23, 733-741.

(18) Irabien, A.; Toquero, A.; Ortiz, M. I. Kinetic behaviour of non-isothermal lime hydration. *Chem. Eng. J.* **1989,** 40, 93-99.

(19) Whitman, W. G.; Davis, G. H. B. The Hydration of Lime. *Ind. Eng. Chem.* **1926,** 18, 118-120.

(20) Schaube, F.; Koch, L.; Wörner, A.; Müller-Steinhagen, H. A thermodynamic and kinetic study of the de- and rehydration of $Ca(OH)_2$ at high H_2O partial pressures for thermo-chemical heat storage. *Thermochim. Acta* **2012,** 538, 9-20.

(21) Lin, S.; Harada, M.; Suzuki, Y.; Hatano, H. CaO Hydration Rate at High Temperature (~1023 K). *Energy Fuels* **2006,** 20, 903-908.

(22) Lin, S.; Wang, Y.; Suzuki, Y. High-Temperature CaO Hydration/$Ca(OH)_2$ Decomposition over a Multitude of Cycles. *Energy Fuels* **2009,** 23, 2855-2861.

(23) Wang, Y.; Lin, S.; Suzuki, Y. Effect of CaO content on hydration rates of Ca-based sorbents at high temperature. *Fuel Process. Technol.* **2008,** 89, 220-226.

(24) Irabien, A.; Viguri, J. R.; Ortiz, I. Thermal dehydration of calcium hydroxide. 1. Kinetic model and parameters. *Ind. Eng. Chem. Res.* **1990,** 29, 1599-1606.

(25) Galwey, A. K.; Laverty, G. M. A kinetic and mechanistic study of the dehydroxylation of calcium hydroxide. *Thermochim. Acta* **1993,** 228, 359-378.

(26) Matsuda, H.; Ishizu, T.; Lee, S. K.; Hasatani, M. Kinetic Study of $Ca(OH)_2$/CaO Reversible Thermochemical Reaction for Thermal Energy Storage by Means of Chemical Reaction. *Kagaku Kogaku Ronbun.* **1985,** 11, 542-548.

(27) Fujii, I.; Ishino, M.; Akiyama, S.; Murthy, M. S.; Rajanandam, K. S. Behavior of $Ca(OH)_2$/CaO pellet under dehydration and hydration. *Sol. Energy* **1994,** 53, 329-341.

(28) Barin, I. *Thermochemical data of pure substances*; VCH Verlagsgesellschaft Weinheim, Germany; New York, 1989.

(29) Nikulshina, V.; Steinfeld, A. CO_2 capture from air via CaO-carbonation using a solar-driven fluidized bed reactor - Effect of temperature and water vapor concentration. *Chem. Eng. J.* **2009,** 155, 867-873.

(30) Samms, J. A. C.; Evans, B. E. Thermal dissociation of $Ca(OH)_2$ at elevated pressures. *J. Appl. Chem.* **1968,** 18, 5-8.

(31) Halstead, P. E.; Moore, A. E. The thermal dissociation of calcium hydroxide. *J. Chem. Soc.* **1957**, 3873-3875.

(32) Vyazovkin, S.; Burnham, A. K.; Criado, J.M.; Pérez-Maqueda, L.A.; Popescu, C.; Sbirrazzuoli, N. ICTAC Kinetics Committee recommendations for performing kinetic computations on thermal analysis data. *Thermochim. Acta* **2011,** 520, 1-19.

(33) Levenspiel, O. *Chemical Reaction Engineering*; John Wiley & Sons: New York, 1999.

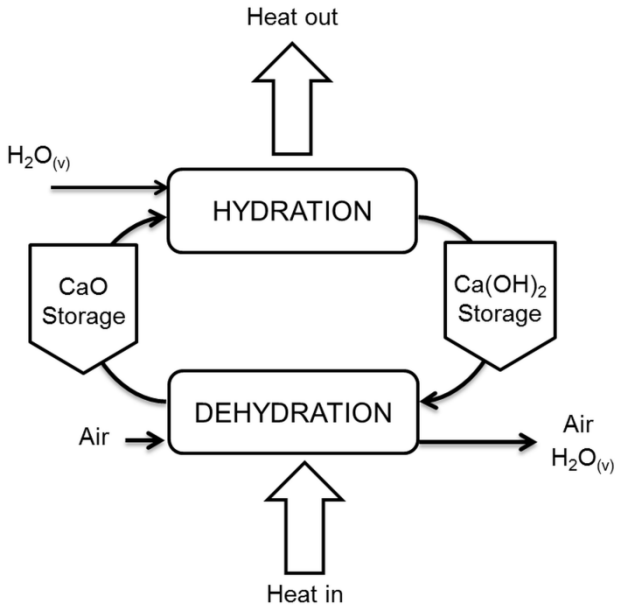

Figure 1. StoRRe $CaO/Ca(OH)_2$ thermochemical energy storage process concept

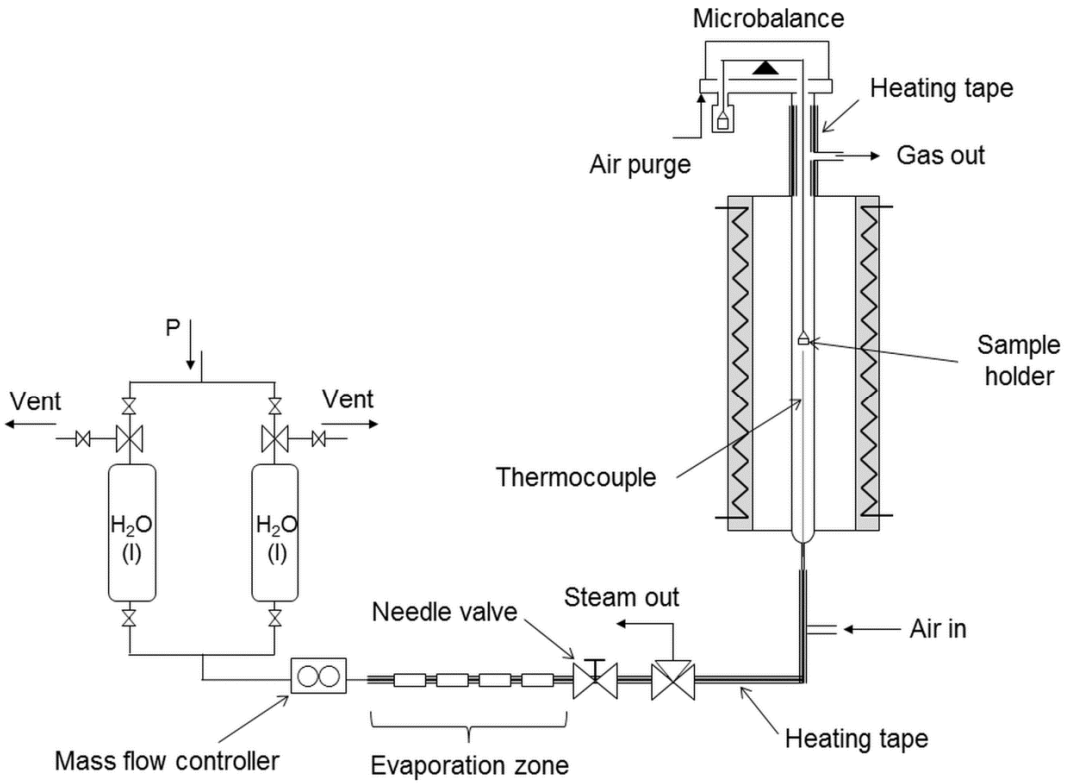

Figure 2. Thermo-gravimetric analyzer and steam generation equipment scheme

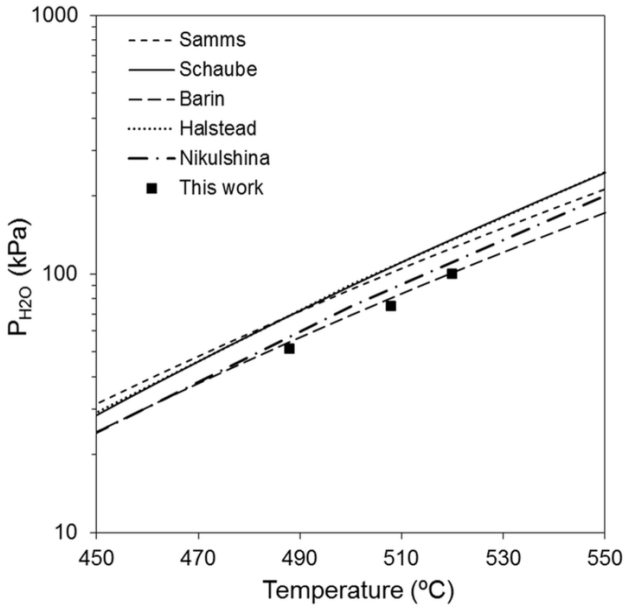

Figure 3. Different $CaO/Ca(OH)_2$ equilibrium curves at the operation conditions range studied in this work

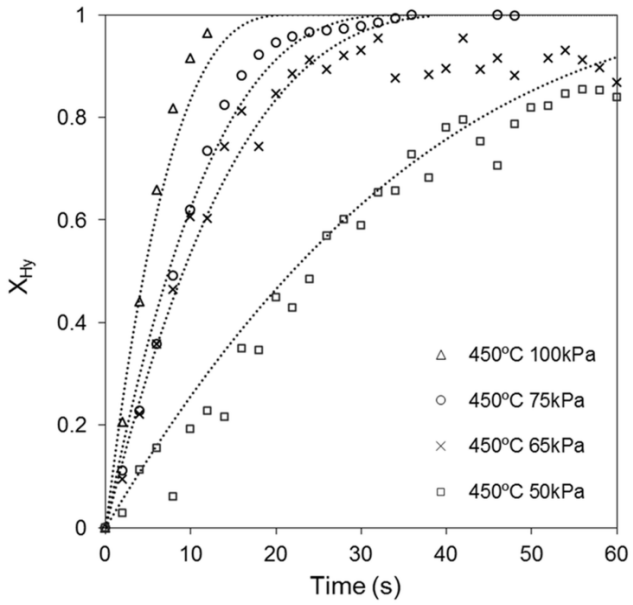

Figure 4. Hydration conversion (X_{Hy}) vs. time, data corresponding to experimental results at 450ºC and four different partial steam pressures (P_{H2O} 100, 75, 65 and 50kPa), using 3mg samples of Compostilla limestone (100-200μm), an initial calcination at 800ºC during 10min and a total gas flow of $7.3\times10^{-6}m^3/s$ (STP)

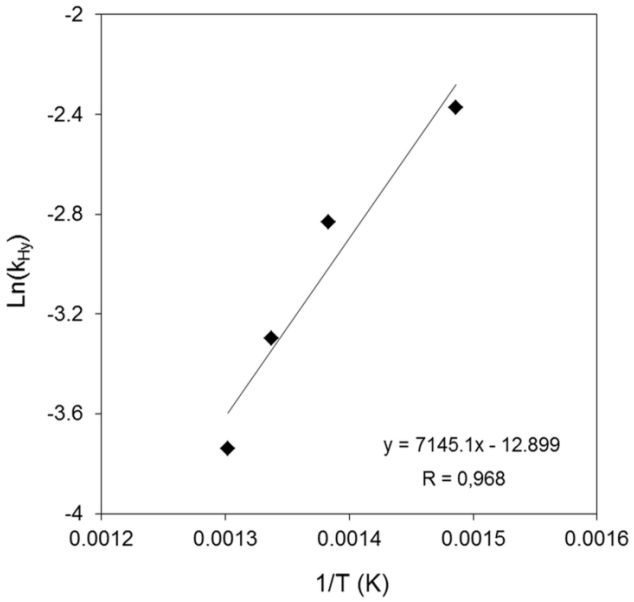

Figure 5. Arrhenius plot for the hydration reaction, corresponding to four different temperatures (400, 450, 475 and 500ºC) and P_{H2O}-Peq=45kPa, using 3mg samples of Compostilla limestone (100-200µm), an initial calcination at 800ºC during 10min and a total gas flow of $7.3\times10^{-6}m^3/s$ (STP)

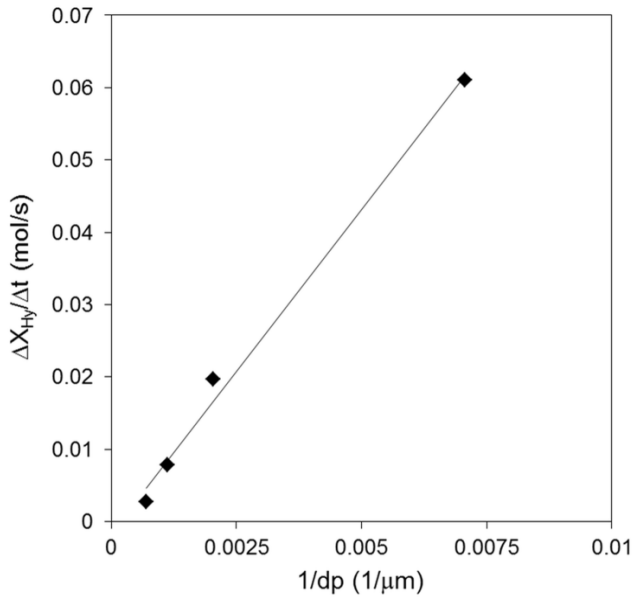

Figure 6. Maximum hydration reaction rate ($\Delta X_{Hy}/\Delta t$ in mol/s) vs. the inverse of the average particle diameter (1/dp in 1/μm) for four particle size cuts, 100-200μm, 400-600μm, 800μm-1mm and 1-2mm, at 450ºC and P_{H2O}=65kPa, using 3mg samples of Compostilla limestone, an initial calcination at 800ºC during 10min and a total gas flow of $7.3\times10^{-6}m^3/s$ (STP)

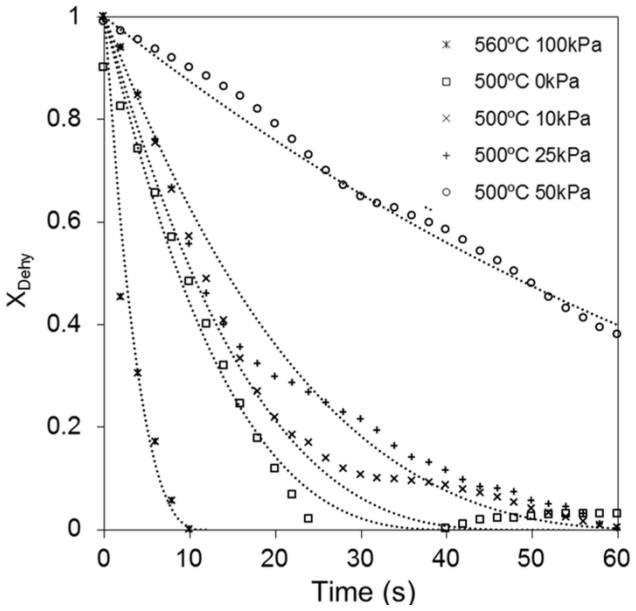

Figure 7. Dehydration conversion (X_{Dehy}) vs. time at 500ºC and four different partial steam pressures (P_{H2O} 0, 10, 25 and 50kPa), and 560ºC and 100kPa, using 3mg samples of Compostilla limestone (100-200μm), an initial calcination at 800ºC during 10min and a total gas flow of $7.3\times10^{-6}m^3/s$ (STP)

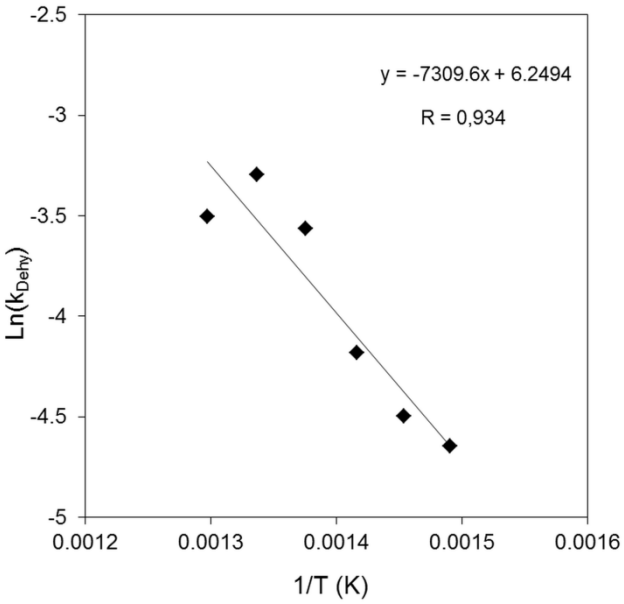

Figure 8. Arrhenius parameters calculation for dehydration reaction for six different temperatures (400, 415, 433, 450, 475 and 500ºC) and P_{H2O} =0kPa, using 3mg samples of Compostilla limestone (100-200µm), an initial calcination at 800ºC during 10min and a total gas flow of $7.3\times10^{-6}m^3/s$ (STP)

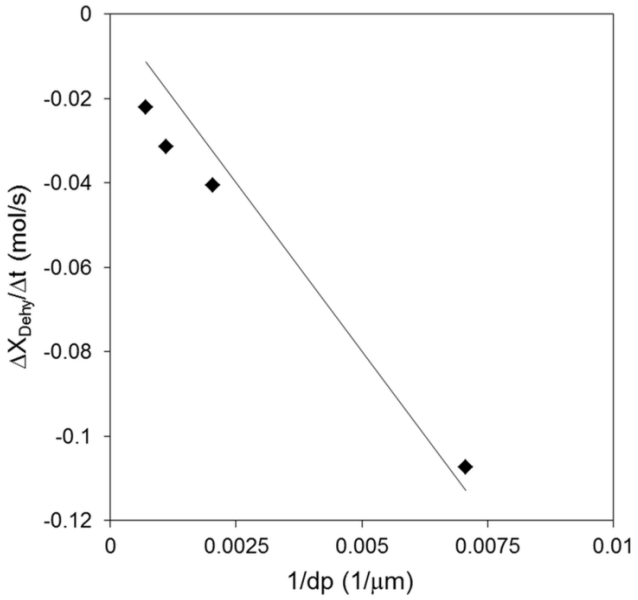

Figure 9. Maximum dehydration reaction rate ($\Delta X_{Dehy}/\Delta t$ in mol/s) vs. the inverse of the average particle diameter (1/dp in 1/μm) for four particle size cuts, 100-200μm, 400-600μm, 800μm-1mm and 1-2mm, at 500ºC and P_{H2O}=0kPa, using 3mg samples of Compostilla limestone, an initial calcination at 800ºC during 10min and a total gas flow of $7.3\times10^{-6}m^3/s$ (STP)

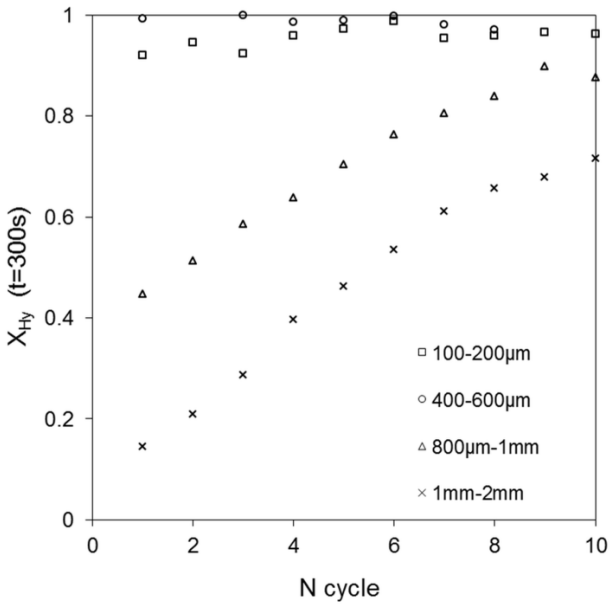

Figure 10. Hydration conversion after 300s (X_{Hy}) vs. the number of hydration – dehydration cycles (N) for four experiments carried out with different particle size cuts: 100-200µm, 400-600µm, 800µm-1mm and 1-2mm, under hydration at 450ºC and P_{H2O}=65kPa and dehydration at 500ºC in air, using 3mg samples of Compostilla limestone, an initial calcination at 800ºC during 10min and a total gas flow of $7.3\times10^{-6}m^3/s$ (STP)